International Journal of Structural Stability and Dynamics
Vol. 15, No. 1 (2015) 1450035 (24 pages)

DOI: 10.1142/S0219455414500357

Moving Force-Induced Vibration of a Rotating Beam with Elastic Boundary Conditions

Binglin Lv* and Wanyou Li†

College of Power and Energy Engineering
Harbin Engineering University, Nangang
Harbin 150001, P. R. China
**lvbinglin@gmail.com*
†*hrbeu_ripet_lwy@163.com*

Huajiang Ouyang‡

School of Engineering, University of Liverpool
The Quadrangle, Liverpool, L69 3GH, UK
and
State Key Laboratory of Structural Analysis for Industrial Equipment
Dalian University of Technology
Dalian 116024, P. R. China
h.ouyang@liverpool.ac.uk

Received 12 March 2014
Accepted 20 May 2014
Published 14 August 2014

In this paper, an analytical technique, the so-called Fourier Spectral method (FSM), is extended to the vibration analysis of a rotating Rayleigh beam considering the gyroscopic effect. The model presented can have arbitrary boundary conditions specified in terms of elastic constraints in the translations and rotations or even in terms of attached lumped masses and inertias. Each displacement function is universally expressed as a linear combination of a standard Fourier cosine series and several supplementary functions introduced to ensure and accelerate the convergence of the series expansion. Lagrange's equation is established for all the unknown Fourier coefficients viewed as a set of independent generalized coordinates. A numerical model is constructed for the rotating beam. First, a numerical example considering simply supported boundary conditions at both ends is calculated and the results are compared with those of a published paper to show the accuracy and convergence of the proposed model. Then, the method is applied to one real work piece structure with elastically supported boundary conditions updated from the modal experiment results including both the frequencies and mode shapes using the method of least squares. Several numerical examples of the updated model are studied to show the effects of some parameters on the dynamic characteristics of the work piece subjected to moving loads at different constant velocities.

Keywords: Rayleigh beam; gyroscopic effect; spectral method; elastic boundary conditions; moving load.

‡Corresponding author.

1. Introduction

Machining has a long history and turning is one of the widely used machining technologies and is carried out on a lathe. As excessive vibration and chatter may occur under certain conditions during a turning process, vibration in metal cutting is familiar to machine tool operators. As a kind of rotating parts in a machine, the dynamic characteristics of the work piece is of vital importance: A high level of rotor vibration not only reduces the machining accuracy of the work piece leading to poor surface quality but also causes damage to the machine or transmit vibration to the supporting structure.[1] Therefore, vibration problems compel a machinist to reduce cutting speeds well below the capacity of a machine or tool. There are several reasons why vibration problem occurs during turning, some of which are related to the vibration characteristics of cutters (nose radius, insert size, entering angle, materials used etc.) and work pieces while others related to the complex interaction at the interface between the work piece and the cutter where especially the regeneration of waviness is encountered.

A work piece is fixed in a lathe which should be regarded as a structure elastically supported at both ends. This means the dynamics of the lathe is also (partly) included when the dynamics of the work piece is studied. The problem of elastically supported beams subjected to moving loads has received little attention.[2,3] The main purpose of this paper is to investigate the effect of complex boundary conditions on the dynamic characteristics of rotating work pieces under moving loads whilst other parts of lathes such as cutters and so on are neglected here. The work piece is modeled as a rotating member subjected to a three-directional moving load.[4] Many researchers have studied the effect of moving loads on the dynamic characteristics of rotating structures.

Katz *et al.*[5] established models of rotating beams based on Euler–Bernoulli, Rayleigh and Timoshenko beam theories with simply supported boundary conditions subject to a load moving at a constant velocity. Xiao and Yang[6] investigated linear and nonlinear dynamic models of a rotating Euler–Bernoulli beam with flexible support as flexible multi-body systems. Kuo and Tu[7] studied the dynamic stability and vibration control for a rotating elastic beam connected with an end mass driven by a direct current motor. Huang and Hsu[8] investigated the resonance of a rotating cylindrical shell excited by harmonic moving loads. A general modal expansion method was adopted to obtain the response of the shell under a harmonic moving load analytically. Lin and Trethewey[9] modeled the moving dynamic loads induced by the movement of a spring-mass-damper system of elastic beams using a finite element formulation. Argento and Scott[10] researched a simply supported Timoshenko beam considering nonconstant load velocity. Argento and Morano[11] studied a spinning pinned–pinned and clamped–clamped Timoshenko beam subjected to an axially accelerating distributed line load of deflection-dependent magnitude. The assumed mode method was used by Lee[12] to express the kinetic and potential energy and then equations of motion were derived by using Hamilton's principle with various

combinations of constant and nonconstant axial speeds of the moving load simulated. Stochastic dynamic response of a rotating simply supported beam subjected to a random force with constant mean value moving at a constant speed along the beam was analyzed by Zibdeh and Juma.[13] El-Saeidy[14] presented the first finite element formulation for the dynamic analysis of a rotating shaft with or without nonlinear boundary conditions under a moving load arising from nonlinear rolling bearings. Yau *et al.*[3] investigated the dynamic response of bridge girders with elastic stiffness at both ends under moving train loads. Wang *et al.*[15] studied the resonance and sub-resonance acceleration response of a two-span continuous railway bridge subjected to moving train loadings. Chen and Tsao[16] analyzed the stability of regenerative chatter in a turning process with the work piece modeled as a cantilever beam. Ouyang and Wang[17] presented a dynamic model for the vibration of a rotating Timoshenko beam subjected to a three-directional moving surface load in the axial direction in which the bending moment to the axial surface load component is included.

A lot of work related to the complex interaction between the cutter and the work piece has been done by researchers. Ganguli *et al.*[18] studied the relationship between instability of regenerative chatter and structural damping, and active damping was included to enhance the stability limits of the system. Insperger *et al.*[19] investigated the nonlinear dynamics of a state-dependent delay model of the turning process which revealed that the Hopf bifurcation depended on the feed rate by modeling the system as a 2 DOF oscillator excited by the cutting force. Litak *et al.*[20] examined the regenerative cutting process of a single DOF nonsmooth model with a friction component and a time delay term. For most of the research, the vibration characteristics of work pieces are not considered in detail or even neglected. Dai and Wang[21] presented one novel methodology with the work piece discretized into finite beam elements and the cutter modeled as one oscillator considering the nonlinear electrical features of the drive motor of machining system. Han *et al.*[22] presented a dynamic model for the vibration in turning operation taking into account the regenerative mechanism with the work piece modeled as a cantilever beam rotating about its longitudinal axis.

In this paper, a rotating beam excited by moving loads is dealt with using the Fourier Spectral method (FSM) which was previously proposed by Li[23] and has also extended to structures such as coupled rectangular plates recently by Du *et al.*[24] The model is meant to approximate the turning of a work piece on a lathe. The objective is not trying to establish an improved metal cutting theory. The rotating work piece during the machining process contains two main parts: The work piece and the spindle with chuck. For simplification, the spindle with chuck is modeled as a lumped mass with 5 DOF attached to the work pieces with several springs. At the other end, several springs are also presented. All the related parameters are obtained based on the model updating theory[25] considering both the frequencies and mode shape data from experiment. After that, the dynamic characteristics of the work piece are analyzed based on the obtained parameters.

2. Dynamic Model

According to the characteristics of the rotating work piece system, it can be modeled as shown in Fig. 1: The work piece itself is represented by a rotating Rayleigh beam while the spindle (with chuck) is simplified as one lumped mass connected to the beam with translational springs k_{yc}, k_{zc} and rotational springs K_{yc}, K_{zc}. As the spindle (with chuck) was also supported by the main body of lathe, two translational springs k_{ym}, k_{zm} and two rotational springs K_{ym}, K_{zm} are included in the model. The work piece is allowed to bend in both the xy and zx planes. Torsional vibration of the work piece is not considered as the first torsional frequency is much higher than the first several bending frequencies. As a result of the complexity of the model, only the parameters contained in the x-y plane are plotted.

Based on the Rayleigh beam theory, the strain energy of the beam system can be expressed as (modified from Ref. 4)

$$\begin{aligned} V = {} & \frac{1}{2}\int_0^l EI\left(\left(\frac{\mathrm{d}^2 v}{\mathrm{d}x^2}\right)^2 + \left(\frac{\mathrm{d}^2 w}{\mathrm{d}x^2}\right)^2\right)\mathrm{d}x \\ & + \frac{1}{2}\left(k_{y0}v^2 + K_{y0}\left(\frac{\mathrm{d}v}{\mathrm{d}x}\right)^2 + k_{z0}w^2 + K_{z0}\left(\frac{\mathrm{d}w}{\mathrm{d}x}\right)^2\right)\Big|_{x=0} \\ & + \frac{1}{2}\left(k_{y1}v^2 + K_{y1}\left(\frac{\mathrm{d}v}{\mathrm{d}x}\right)^2 + k_{z1}w^2 + K_{z1}\left(\frac{\mathrm{d}w}{\mathrm{d}x}\right)^2\right)\Big|_{x=l} \\ & - \frac{1}{2}\int_s^l P_x\left(\left(\frac{\mathrm{d}v}{\mathrm{d}x}\right)^2 + \left(\frac{\mathrm{d}w}{\mathrm{d}x}\right)^2\right)\mathrm{d}x, \end{aligned} \tag{1}$$

where l is the beam length, and s is the instantaneous horizontal location of the moving force; v and w are the flexural displacements of the neutral axis in the two perpendicular directions in the plane of the beam's circular cross section, E and I are, respectively, the Young's modulus and the moment of area; k_{y0}, k_{z0}, k_{y1} and k_{z1} are the linear spring constants, and K_{y0}, K_{z0}, K_{y1} and K_{z1} are the rotational spring constants at $x = 0$ and $x = l$, respectively, x is the longitudinal coordinate of the beam.

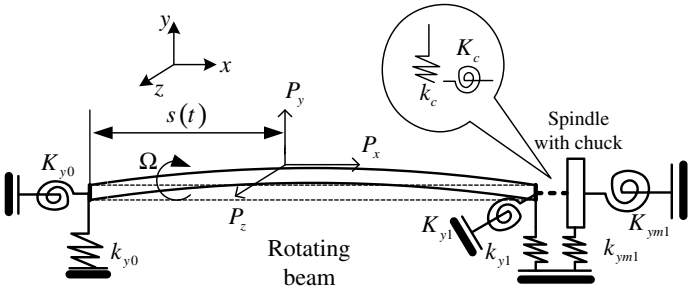

Fig. 1. Rotating parts subjected to a moving load with three perpendicular forces.

The kinetic energy of the rotating beam system will then be

$$T_s = \frac{1}{2}\int_0^l I_d\left(\frac{\partial^2 v}{\partial x \partial t}\right)^2 \mathrm{d}x + \frac{1}{2}\int_0^l I_d\left(\frac{\partial^2 w}{\partial x \partial t}\right)^2 \mathrm{d}x + \frac{1}{2}\int_0^l \rho A\left(\frac{\partial v}{\partial t}\right)^2 \mathrm{d}x + \frac{1}{2}\int_0^l \rho A\left(\frac{\partial w}{\partial t}\right)^2 \mathrm{d}x + \frac{1}{2}\Omega I_p \int_0^l \left(\frac{\partial w}{\partial t}\frac{\partial^2 v}{\partial x \partial t} - \frac{\partial v}{\partial t}\frac{\partial^2 w}{\partial x \partial t}\right)\mathrm{d}x + \frac{1}{2}\Omega^2 I_p l, \quad (2)$$

where $I_d = \rho A r^2/4$, $I_p = 2I_d$, $\theta_v = \mathrm{d}v/\mathrm{d}x$, $\theta_w = \mathrm{d}w/\mathrm{d}x$, ρ is the density, r is the radius of the shafting, Ω is the constant angular speed of the work piece rotating about the longitudinal axis.

The virtual work done by forces P_y, P_z, and moment M_z is

$$\delta W = P_y \delta v(s,t) + P_z \delta w(s,t) + M_z \frac{\partial \delta w}{\partial x}\bigg|_{x=s}, \quad (3)$$

where, the bending moment M_z is resulted from the translation of the axial force P_x as

$$M_z = -P_x r. \quad (4)$$

As previously done for beam and rectangular plate,[23,24] the displacement will be sought as

$$v(x) = \sum_{m=0}^{\infty} A_m \cos \lambda_{lm} x + \sum_{k=1}^{4} (C_k \xi_l^k(x)) = \boldsymbol{\Psi}^{\mathrm{T}} \boldsymbol{\alpha}, \quad (5)$$

$$w(x) = \sum_{m=0}^{\infty} B_m \cos \lambda_{lm} x + \sum_{k=1}^{4} (D_k \xi_l^k(x)) = \boldsymbol{\Psi}^{\mathrm{T}} \boldsymbol{\beta}, \quad (6)$$

where

$$\xi_l^1(x) = \frac{9l}{4\pi}\sin\left(\frac{\pi x}{2l}\right) - \frac{l}{12\pi}\sin\left(\frac{3\pi x}{2l}\right), \quad (7a)$$

$$\xi_l^2(x) = -\frac{9l}{4\pi}\cos\left(\frac{\pi x}{2l}\right) - \frac{l}{12\pi}\cos\left(\frac{3\pi x}{2l}\right), \quad (7b)$$

$$\xi_l^3(x) = \frac{l^3}{\pi^3}\sin\left(\frac{\pi x}{2l}\right) - \frac{l^3}{3\pi^3}\sin\left(\frac{3\pi x}{2l}\right), \quad (7c)$$

$$\xi_l^4(x) = -\frac{l^3}{\pi^3}\cos\left(\frac{\pi x}{2l}\right) - \frac{l^3}{3\pi^3}\cos\left(\frac{3\pi x}{2l}\right), \quad (7d)$$

and

$$\boldsymbol{\Psi} = \{\cos\lambda_{l1}x, \ldots, \cos\lambda_{lN}x, \xi_l^1(x), \xi_l^2(x), \xi_l^3(x), \xi_l^4(x)\}^{\mathrm{T}},$$
$$\boldsymbol{\alpha} = \{A_0, A_1, \ldots, A_N, C_1, \ldots, C_4\}^{\mathrm{T}},$$
$$\boldsymbol{\beta} = \{B_0, B_1, \ldots, B_N, D_1, \ldots, D_4\}^{\mathrm{T}}.$$

Using Eqs. (5)–(7), Eqs. (1) and (2) can then be rewritten as

$$\begin{aligned} V = & \frac{1}{2}\int_0^l EI(\boldsymbol{\alpha}^{\mathrm{T}}\boldsymbol{\Psi}''\boldsymbol{\Psi}''^{\mathrm{T}}\boldsymbol{\alpha} + \boldsymbol{\beta}^{\mathrm{T}}\boldsymbol{\Psi}''\boldsymbol{\Psi}''^{\mathrm{T}}\boldsymbol{\beta})\mathrm{d}x \\ & + \frac{1}{2}(k_{x0}\boldsymbol{\alpha}^{\mathrm{T}}\boldsymbol{\Psi}\boldsymbol{\Psi}^{\mathrm{T}}\boldsymbol{\alpha} + K_{x0}\boldsymbol{\alpha}^{\mathrm{T}}\boldsymbol{\Psi}'\boldsymbol{\Psi}'^{\mathrm{T}}\boldsymbol{\alpha} + k_{y0}\boldsymbol{\beta}^{\mathrm{T}}\boldsymbol{\Psi}\boldsymbol{\Psi}^{\mathrm{T}}\boldsymbol{\beta} + K_{y0}\boldsymbol{\beta}^{\mathrm{T}}\boldsymbol{\Psi}'\boldsymbol{\Psi}'^{\mathrm{T}}\boldsymbol{\beta})\Big|_{x=0} \\ & + \frac{1}{2}(k_{x1}\boldsymbol{\alpha}^{\mathrm{T}}\boldsymbol{\Psi}\boldsymbol{\Psi}^{\mathrm{T}}\boldsymbol{\alpha} + K_{x1}\boldsymbol{\alpha}^{\mathrm{T}}\boldsymbol{\Psi}'\boldsymbol{\Psi}'^{\mathrm{T}}\boldsymbol{\alpha} + k_{y1}\boldsymbol{\beta}^{\mathrm{T}}\boldsymbol{\Psi}\boldsymbol{\Psi}^{\mathrm{T}}\boldsymbol{\beta} + K_{y1}\boldsymbol{\beta}^{\mathrm{T}}\boldsymbol{\Psi}'\boldsymbol{\Psi}'^{\mathrm{T}}\boldsymbol{\beta})\Big|_{x=l} \\ & - \frac{1}{2}\int_s^l P_x(\boldsymbol{\alpha}^{\mathrm{T}}\boldsymbol{\Psi}'\boldsymbol{\Psi}'^{\mathrm{T}}\boldsymbol{\alpha} + \boldsymbol{\beta}^{\mathrm{T}}\boldsymbol{\Psi}'\boldsymbol{\Psi}'^{\mathrm{T}}\boldsymbol{\beta})\mathrm{d}x, \end{aligned} \tag{8}$$

$$\begin{aligned} T_s = & \frac{1}{2}\int_0^l I_d\dot{\boldsymbol{\alpha}}^{\mathrm{T}}\boldsymbol{\Psi}'\boldsymbol{\Psi}'^{\mathrm{T}}\dot{\boldsymbol{\alpha}}\mathrm{d}x + \frac{1}{2}\int_0^l I_d\dot{\boldsymbol{\beta}}^{\mathrm{T}}\boldsymbol{\Psi}'\boldsymbol{\Psi}'^{\mathrm{T}}\dot{\boldsymbol{\beta}}\mathrm{d}x \\ & + \frac{1}{2}\int_0^l \rho A\dot{\boldsymbol{\alpha}}^{\mathrm{T}}\boldsymbol{\Psi}\boldsymbol{\Psi}^{\mathrm{T}}\dot{\boldsymbol{\alpha}}\mathrm{d}x + \frac{1}{2}\int_0^l \rho A\dot{\boldsymbol{\beta}}^{\mathrm{T}}\boldsymbol{\Psi}\boldsymbol{\Psi}^{\mathrm{T}}\dot{\boldsymbol{\beta}}\mathrm{d}x \\ & + \frac{1}{2}\Omega I_p\int_0^l(\boldsymbol{\alpha}^{\mathrm{T}}\boldsymbol{\Psi}'\boldsymbol{\Psi}'^{\mathrm{T}}\dot{\boldsymbol{\beta}} - \boldsymbol{\beta}^{\mathrm{T}}\boldsymbol{\Psi}'\boldsymbol{\Psi}'^{\mathrm{T}}\dot{\boldsymbol{\alpha}})\mathrm{d}x + \frac{1}{2}\Omega^2 J_p, \end{aligned} \tag{9}$$

where the over dot represents the derivative with respect to time t and the prime represents the derivative with respect to x.

Lagrange's equations of motion can then be obtained

$$\begin{aligned} & \left(I_d\int_0^l \boldsymbol{\Psi}'\boldsymbol{\Psi}'^{\mathrm{T}}\mathrm{d}x + \rho A\int_0^l \boldsymbol{\Psi}\boldsymbol{\Psi}^{\mathrm{T}}\mathrm{d}x\right)\ddot{\boldsymbol{\alpha}} + \Omega I_p\int_0^l(\boldsymbol{\Psi}'\boldsymbol{\Psi}'^{\mathrm{T}})\mathrm{d}x\dot{\boldsymbol{\beta}} \\ & \quad + \left(EI\int_0^l \boldsymbol{\Psi}''\boldsymbol{\Psi}''^{\mathrm{T}}\mathrm{d}x + (k_{x0}\boldsymbol{\Psi}\boldsymbol{\Psi}^{\mathrm{T}} + K_{x0}\boldsymbol{\Psi}'\boldsymbol{\Psi}'^{\mathrm{T}})\Big|_{x=0}\right. \\ & \quad \left. + (k_{x1}\boldsymbol{\Psi}\boldsymbol{\Psi}^{\mathrm{T}} + K_{x1}\boldsymbol{\Psi}'\boldsymbol{\Psi}'^{\mathrm{T}})\Big|_{x=l} - P_x\int_s^l \boldsymbol{\Psi}'\boldsymbol{\Psi}'^{\mathrm{T}}\mathrm{d}x\right)\boldsymbol{\alpha} \\ & = P_y\boldsymbol{\Psi}^{\mathrm{T}}|_{x=s} - P_x r\boldsymbol{\Psi}'^{\mathrm{T}}|_{x=s}, \end{aligned} \tag{10}$$

$$\begin{aligned} & \left(I_d\int_0^l \boldsymbol{\Psi}'\boldsymbol{\Psi}'^{\mathrm{T}}\mathrm{d}x + \rho A\int_0^l \boldsymbol{\Psi}\boldsymbol{\Psi}^{\mathrm{T}}\mathrm{d}x\right)\ddot{\boldsymbol{\beta}} - \Omega I_p\int_0^l \boldsymbol{\Psi}'\boldsymbol{\Psi}'^{\mathrm{T}}\mathrm{d}x\dot{\boldsymbol{\alpha}} \\ & \quad + \left(EI\int_0^l \boldsymbol{\Psi}''\boldsymbol{\Psi}''^{\mathrm{T}}\mathrm{d}x + (k_{y0}\boldsymbol{\Psi}\boldsymbol{\Psi}^{\mathrm{T}} + K_{y0}\boldsymbol{\Psi}'\boldsymbol{\Psi}'^{\mathrm{T}})\Big|_{x=0}\right. \\ & \quad \left. + (k_{y1}\boldsymbol{\Psi}\boldsymbol{\Psi}^{\mathrm{T}} + K_{y1}\boldsymbol{\Psi}'\boldsymbol{\Psi}'^{\mathrm{T}})\Big|_{x=l} - P_x\int_s^l \boldsymbol{\Psi}'\boldsymbol{\Psi}'^{\mathrm{T}}\mathrm{d}x\right)\boldsymbol{\beta} \\ & = P_z\boldsymbol{\Psi}^{\mathrm{T}}|_{x=s}. \end{aligned} \tag{11}$$

The other components in Fig. 1, the kinetic energy for the spindle and the strain energy for the springs can be expressed as

$$T_{\text{spindle}} = \frac{1}{2} m_m (\dot{v}_m^2 + \dot{w}_m^2) + \frac{1}{2} J_d (\dot{\theta}_{ym}^2 + \dot{\theta}_{zm}^2) + \frac{1}{2} J_p (\Omega^2 - 2\Omega \dot{\theta}_{zm} \theta_{ym}) \tag{12}$$

and

$$\begin{aligned} V_{\text{spindle}} = & \frac{1}{2} k_{cy} (\boldsymbol{\Psi}^{\mathrm{T}} \boldsymbol{\alpha}|_{x=l} - v_m)^2 + \frac{1}{2} k_{cz} (\boldsymbol{\Psi}^{\mathrm{T}} \boldsymbol{\beta}|_{x=l_i} - w_m)^2 \\ & + \frac{1}{2} K_c (\boldsymbol{\Psi}'^{\mathrm{T}} \boldsymbol{\alpha}|_{x=l} - \theta_{ym})^2 + \frac{1}{2} K_c (\boldsymbol{\Psi}'^{\mathrm{T}} \boldsymbol{\beta}|_{x=l} - \theta_{zm})^2, \end{aligned} \tag{13}$$

where m_m is the mass of the spindle and $\dot{v}_m$ and $\dot{w}_m$ are the velocities of the spindle in the y and z directions, respectively; $\dot{\theta}_{ym}$ and $\dot{\theta}_{zm}$ are the instantaneous angular velocities about the x and y axes which are fixed on the spindle and rotate with it; J_d and J_p are the diametrical moment of inertia about the shaft line and polar moment of inertia about any axis perpendicular to the shaft line.

With Eqs. (10)–(13), the final equations of motion can then be expressed in a matrix form as,

$$\mathbf{M}\ddot{\mathbf{q}} + \Omega \mathbf{G}\dot{\mathbf{q}} + (\mathbf{K} + \mathbf{K}_p(t))\mathbf{q} = \mathbf{F}(t), \tag{14}$$

where $\mathbf{q} = \{\boldsymbol{\alpha}^{\mathrm{T}}, \boldsymbol{\beta}^{\mathrm{T}}, v_m, w_m, \theta_{ym}, \theta_{zm}\}^{\mathrm{T}}$. The detailed matrix information can be seen in Appendix A.

3. Numerical Results and Discussion

First, in order to compare with the numerical results from the literature, the material and geometrical properties for the first example are taken from Ref. 4. The related beam parameters are as follows: $l = 1\,\text{m}$, $E = 2.07 \times 10^{11}\,\text{Pa}$, and $\rho = 7700\,\text{Kg m}^{-3}$. In this example, Eqs. (5) and (6) are truncated to $N = 10$, respectively. The numerical results of the dynamic responses in terms of the instantaneous relative deflection v_p/v_s at the location of the moving load are given, where v_p is the deflection at the point of the moving load and v_s is the static deflection of the stationary beam at $x = l/2$ when the moving load is applied at the same point as the static load. Nondimensional parameter of $\beta = \pi r/2l$ is used, and $\Omega = 2.5\omega_1$ in which $\omega_1 = (\pi/l)^2\sqrt{El\rho A}$ is the fundamental frequency of the stationary beam. Reasonable values of $P_x = 600\,\text{N}$, $P_y = -300\,\text{N}$, $P_z = -1000\,\text{N}$ are used. The boundary conditions for the rotating beam in Ref. 4 are simply supported at both ends. For this example, such boundary conditions can be simulated by setting all the linear springs to a very big number while the other rotational springs to zero, say, $k_{y0} = k_{z0} = k_{y1} = k_{z1} = 10^{10}$ and $K_{y0} = K_{z0} = K_{y1} = K_{z1} = 0$. The Newmark method (with $\beta = 0.25$ and $\gamma = 0.5$) is used in this paper. In Figs. 2 and 3, the numerical results of v_p/v_s are plotted at velocity $u = 2\,\text{m/s}$ of two radii $r = 0.095\,\text{m}$ and $0.019\,\text{m}$, respectively.

By comparing with the results from Ref. 4, it is shown that the present method can be applied to the moving load problems. It can be clearly observed from the

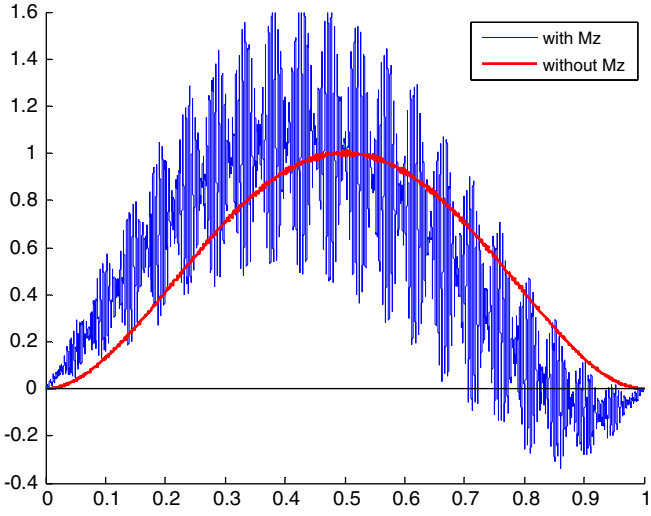

Fig. 2. Dynamic response obtained using realistic speed and axial cutting force with $u = 2\,\mathrm{m/s}$ and $r = 0.095\,\mathrm{m}$.

figure that the phenomenon that the moment would amplify the contributions of the higher harmonics is also observed. By comparing these two figures, it can be easily found that the fluctuation is lower for the shaft with a smaller radius. This can be explained via looking at Eq. (4): with a smaller radius, the shaft would also experience a smaller moving bending moment $(-P_x r)$, which is the main reason for these fluctuations.

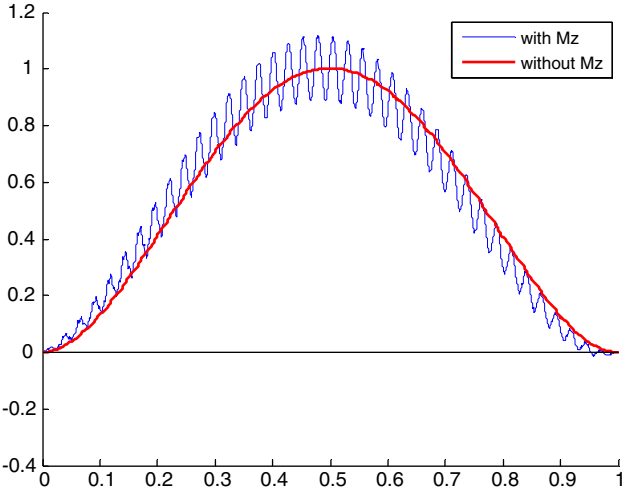

Fig. 3. Dynamic response obtained using realistic speed and axial cutting force with $u = 2\,\mathrm{m/s}$ and $r = 0.019\,\mathrm{m}$.

3.1. *Model updating of the work piece*

Inevitably, there always exist some differences between a real structure or machine and the theoretical model due to the assumptions used in the development of the mathematical model and inaccurate structural properties used in the model.[25] For analyzing the dynamic characteristics of the work piece which is more or less elastically supported, classical boundaries such as simply-supported or clamped–clamped ones, are not enough. In model updating, the correct model must be used and the corresponding sensitive parameters be selected. As for the work piece shown in Fig. 4, the spindle (with chuck) should also be included in the dynamic analysis of the rotating beam as it would also rotate with the work piece. Besides, the tail stock is also elastic. In this paper, the spindle with chuck is modeled as one rigid body with mass m_s and inertia I_s in two directions y and z; and the tail stock is modeled as linear springs.

The connection between the beam and the spindle is modeled as two linear springs and two rotational springs: k_{cy}, K_{cy} and k_{cz}, K_{cz}. As the spindle is supported by bearings, the connection between the spindle and its support is also represented by four springs: k_{cy}, K_{cy} and k_{cz}, K_{cz} in the y and z directions. The connection between the beam and the tailstock is at the center of the cross section which is called the dead center. So it is difficult to transfer any moment between the beam and the tailstock via such a small point (dead center) contact; therefore, the rotational springs are neglected and only two translational springs are added between the tailstock and the beam. It should be said that at the chuck end of the work piece, a length of around 5 mm is inserted into the work piece holder. The connection between the beam and the holder is presented by two translational springs and two rotational springs. For this lathe, those two translational springs are set to be infinite, which is verified in the following model updating procedure. Modal testing on the work piece in the lathe provides measured frequencies and modes required in model updating.

The work piece modeled as a single Rayleigh beam has the following properties: $l = 0.5\,\text{m}$, $E = 2.04 \times 10^{11}$ Pa, and $\rho = 7817.4\,\text{Kg m}^{-3}$, radius $r = 0.018515\,\text{m}$. The

Fig. 4. Rotating part of the turning machine.

spindle with chuck is simplified as lumped mass with $m_m = 26\,\text{Kg}$, $J_d = 0.22\,\text{Kg m}^2$ and $J_p = 0.44\,\text{Kg m}^2$. Two modal tests were performed both in the horizontal plane (x-z) and vertical plane (x-y) to update all the unknown spring constants: k_{y0}, K_{cy}, k_{ym1}, K_{ym1} in the x-y plane and $k_{z0}, K_{cz}, k_{zm1}, K_{zm1}$ in the x-z plane. The theoretical and experimental modes must be paired correctly when comparing two sets of frequencies. For comparing experimental results of the work piece with predicted results by the FSM on the stationary beam, the modal assurance criterion (MAC) is used here[25]:

$$\text{MAC}_{jk} = \frac{(\boldsymbol{\Psi}_{mj}{}^{\text{T}}\boldsymbol{\Psi}_{ak})^2}{(\boldsymbol{\Psi}_{ak}{}^{\text{T}}\boldsymbol{\Psi}_{ak})(\boldsymbol{\Psi}_{mj}{}^{\text{T}}\boldsymbol{\Psi}_{mj})}, \tag{15}$$

where $\boldsymbol{\Psi}_{mj}$ is the measured mode and $\boldsymbol{\Psi}_{ak}$ the analytical mode. The MAC is often used to pair mode shapes derived from analytical models with those obtained experimentally. It is easy to apply and does not require an estimate of the system matrices.

Then the model updating problem can therefore be cast as

$$\min_{\mathbf{x}} \sum_{h=1}^{n} \left\{ \alpha_h \left\| \frac{\lambda_h(\mathbf{x}) - \lambda_{mh}}{\lambda_h(\mathbf{x})} \right\|_2^2 + \beta_h \|1 - \text{MAC}_{hh}(\mathbf{x})\|_2^2 \right\}, \tag{16}$$

where $\mathbf{x}$ is the vector containing all unknown parameters, λ_h is the kth analytical frequency, and λ_{mh}, the kth measured frequency, α_h and β_h are positive scalars to weigh each hth single frequency and mode. In this example, the first five frequencies and modes are used to update these four parameters. Based on a nonlinear programming method, one possible optimum is found for these four parameters: $k_{z0} = 2.06\text{e}10\,\text{N/m}$, $K_{cz} = 4.47\text{e}4\,\text{Nm/rad}$, $k_{zm1} = 7.21\text{e}7\,\text{N/m}$, $K_{zm1} = 4.34\text{e}5\,\text{Nm/rad}$. The comparison between the first five frequencies calculated using these four updated parameters with those from experiment is shown in Table 1.

From this table, it can be seen that the errors of the first five frequencies are very small, especially for the first three frequencies. As for the MAC calculated between the numerical results and the experimental results, only the fifth MAC is smaller than 0.8, which is reasonable; for higher order modes, the error from the test would be greater without the increase in the number of sensors used, and thus, the measured mode

Table 1. Comparison of the first five modes between the numerical results and the experimental results.

	Natural frequency (Hz)			
Modes	Experimental (Hz)	Numerical (Hz)	Difference (%)	MAC
1	229	229.7	−0.31	0.823
2	252	251.8	0.07	0.933
3	337	342.1	−1.50	0.851
4	1280	1218.4	5.06	0.879
5	2740	2672.4	2.53	0.434

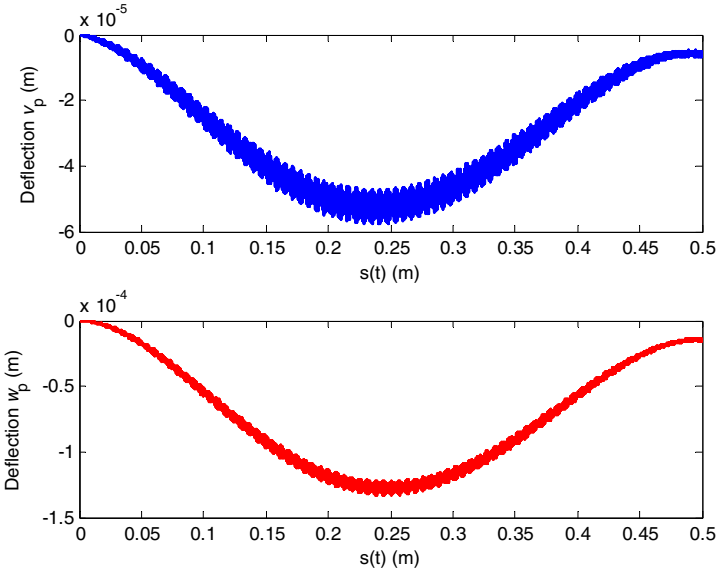

(a)

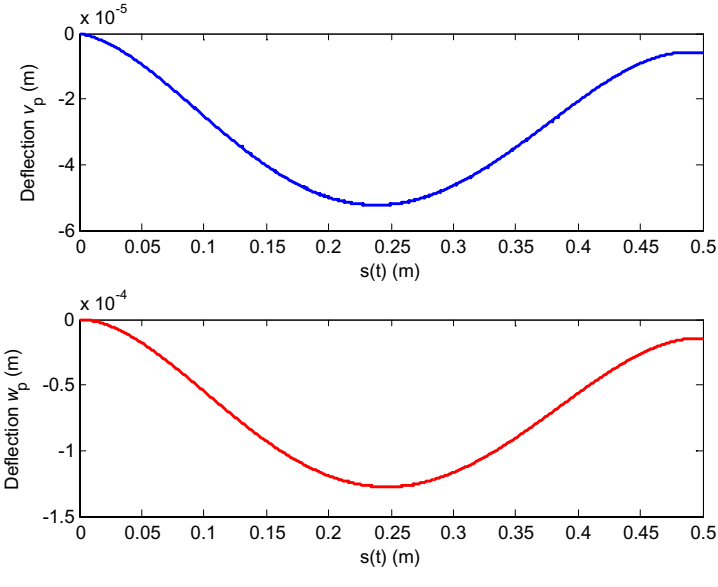

(b)

Fig. 5. Dynamic response of the rotating shaft considering elastically supported boundary conditions subjected to moving load at $u = 6.25\,\mathrm{mm/s}$: (a) Zero initial condition considered; (b) initial static deflection considered and (c) FFT of the response w at the middle point of the shaft.

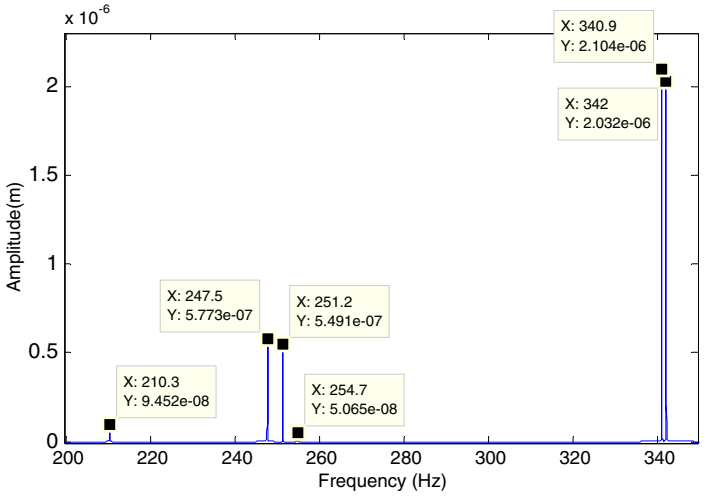

(c)

Fig. 5. (*Continued*)

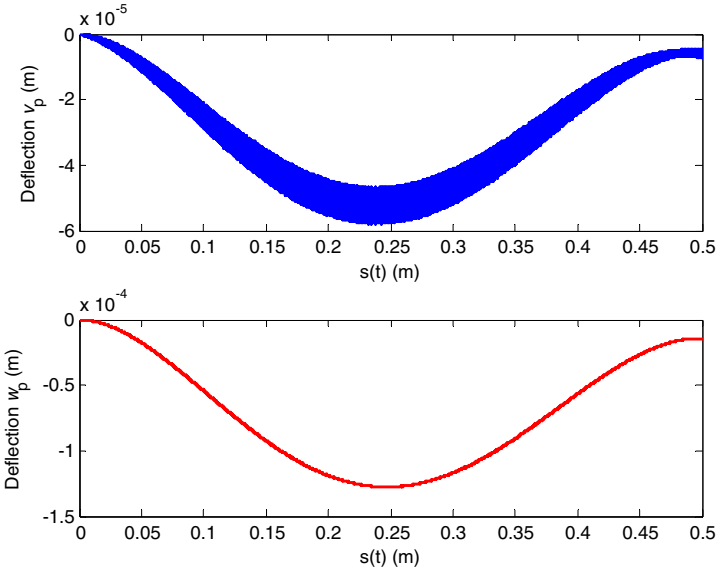

(a)

Fig. 6. Dynamic response of the shaft considering elastically supported boundary conditions subjected to moving load at $u = 6.25\,\text{mm/s}$ (without considering the gyroscopic effect): (a) Zero initial condition considered; (b) initial static deflection considered and (c) FFT of the response w at the middle point of the shaft.

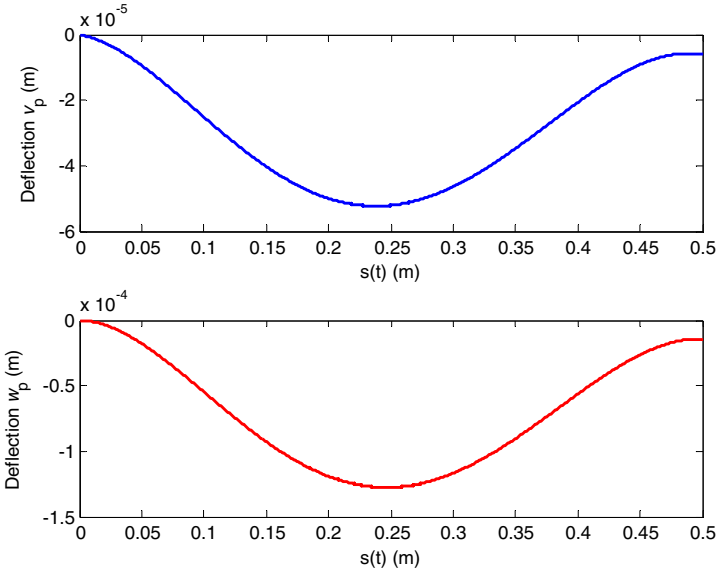

(b)

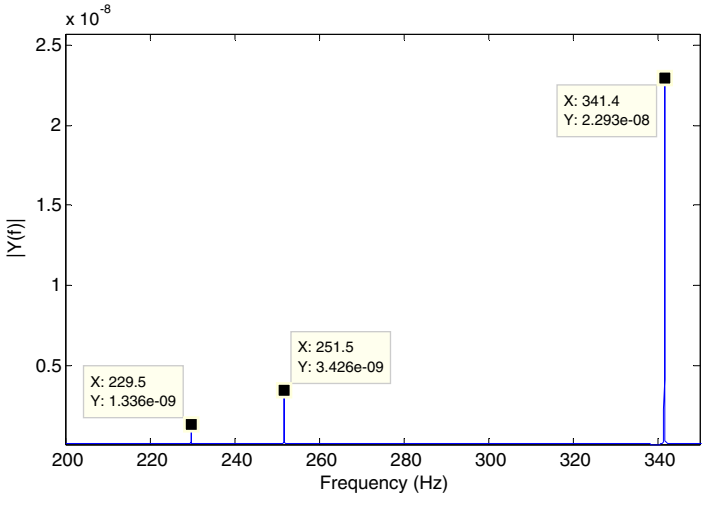

(c)

Fig. 6. (*Continued*)

shape could become less reliable. Other sources of errors include the assumption that other parts of the lathe are rigid. Despite the above errors, approximately, the mathematical model obtained through model updating can be used to simulate the dynamic characteristics of the beam system subjected to moving load.

3.2. *Numerical results based on the updated parameters*

With the updated model, some more numerical examples are presented considering a constant moving load. As this paper is mainly focused on work pieces with elastic boundary conditions, the fluctuation of the cutting depth h is neglected and the three force components applied to the work piece are considered constant here. The following values of cutting forces measured from Test No. 1 reported in Ref. 22 are used: $P_x = 391\,\text{N}$, $P_y = -428\,\text{N}$, and $P_z = -1046\,\text{N}$. Apparently, the responses of the system are mainly affected by two causes: The initial conditions and the moving loads. Here, two different initial conditions are considered: (1) zero displacements and velocities and (2) nonzero initial static displacement obtained with the forces at the starting time $t = 0$ applied to the beam at $x = 0$. Dynamic response of the work piece subjected to three force components and the induced bending moment M_z moving at different speeds are plotted below.

In Fig. 5, response of the work piece subjected to the moving load at $u = 6.25\,\text{mm/s}$ is presented. In Fig. 5(a), it can be seen that the response fluctuates at relatively high frequencies when the initial displacements and velocities are set to be zero. In this example, at $t = 0$, as zero displacements and velocities are included; the effect of the forces behaves as if it is suddenly applied to the beam as impact. In order to study such a kind of impact, static deflection of the beam system with the initial force at $t = 0$ applied at $x = 0$ is calculated and included as the initial displacements. Results under such an initial condition are shown in Fig. 5(b). In order to understand the effect of the initial conditions to the dynamic response of the beam, free vibration of the beam system with the initial displacement set to be the static deflection in Fig. 5(b) are also calculated as shown in Fig. 5(c). It can be seen that the response with higher frequencies in Fig. 5(a) disappears significantly in Fig. 5(b). In Fig. 6, the responses of the work piece neglecting the gyroscopic effect are also given; the fluctuation in the z direction has disappeared. Generally speaking, for Rayleigh Beams, the displacements in the y direction and z direction are independent from each other when the gyroscopic effect is neglected. As the bending moment is only applied in the xy plane and the fluctuation is mainly caused by the moving moment M_z, it should be clear that the fluctuation in the z direction vanishes when gyroscopic coupling is absent. For thorough understanding of the effect of rotating,

Table 2. The first six natural frequencies of the work piece with and without considering gyroscopic effect.

	Natural frequencies (Hz)	
Modes	With gyroscopic effect	Without gyroscopic effect
1	210.4	229.7
2	247.8	229.7
3	251.5	251.8
4	254.9	251.8
5	341.6	342.1
6	342.7	342.1

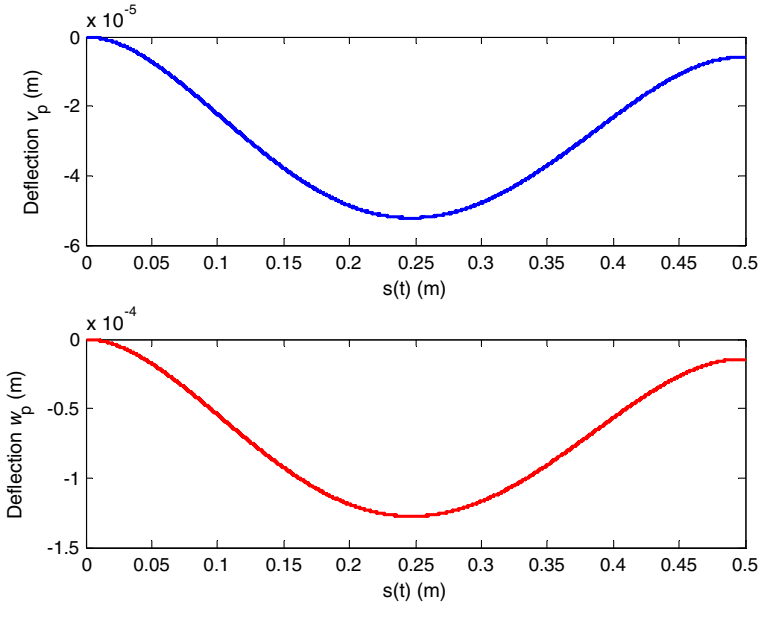

(a)

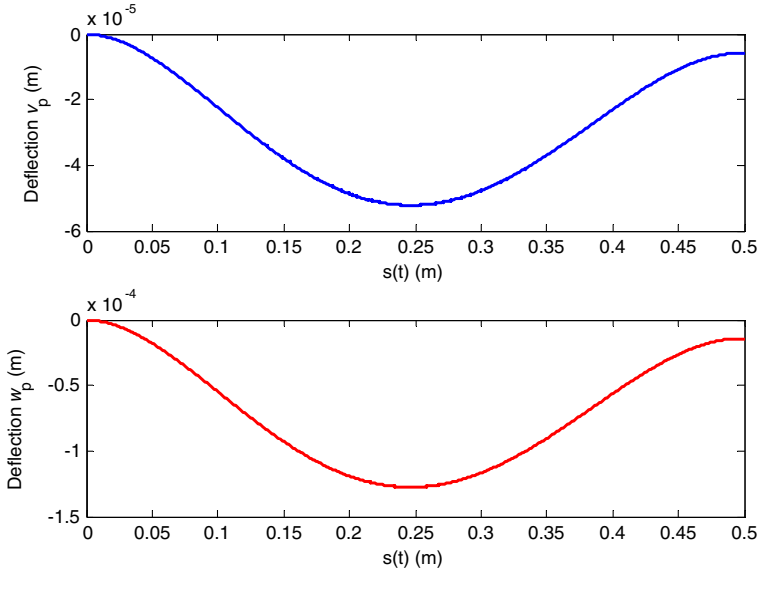

(b)

Fig. 7. Dynamic response of the rotating shaft considering elastically supported boundary conditions subjected to moving load at $u = 6.25$ mm/s (without considering the bending moment M_z): (a) Zero initial condition considered and (b) initial static deflection considered.

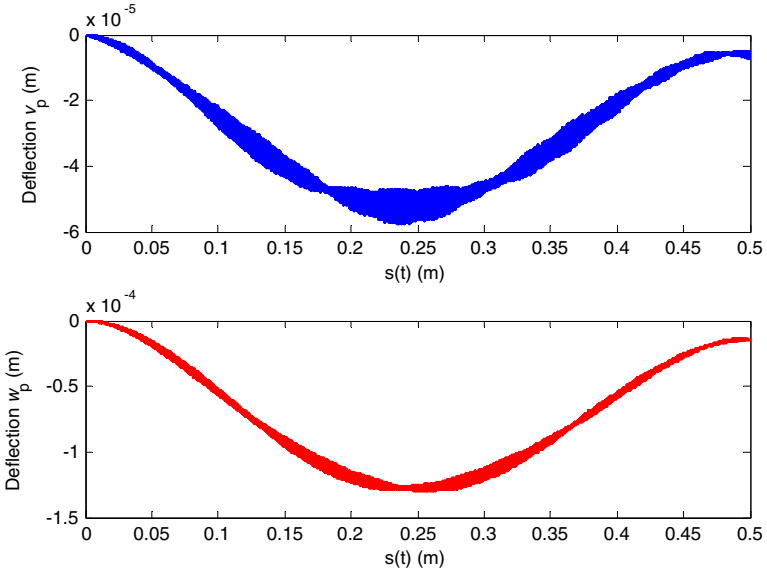

(a)

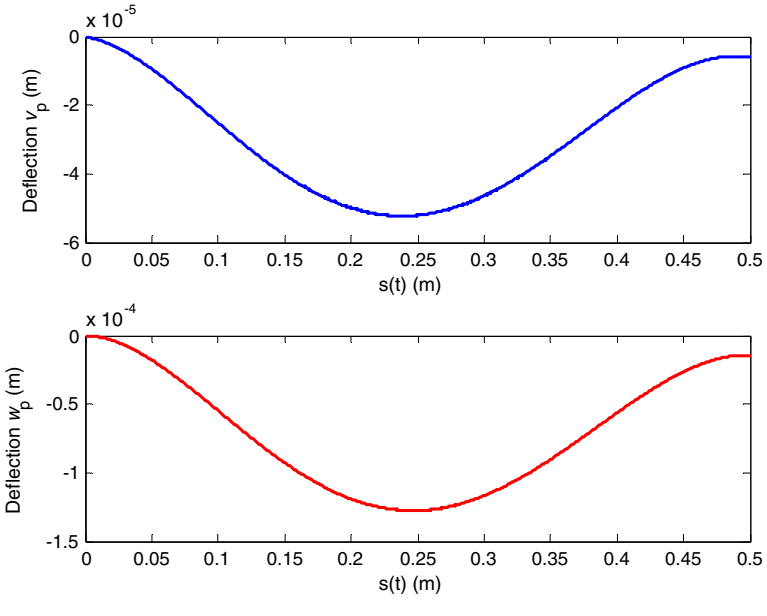

(b)

Fig. 8. Dynamic response of the rotating shaft considering elastically supported boundary conditions subjected to moving load at $u = 125\,\text{mm/s}$: (a) Zero initial condition considered and (b) initial static deflection considered.

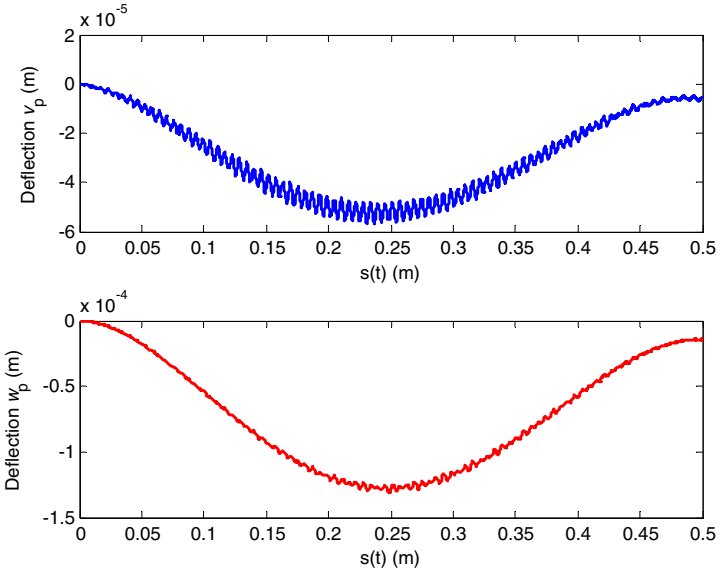

(a)

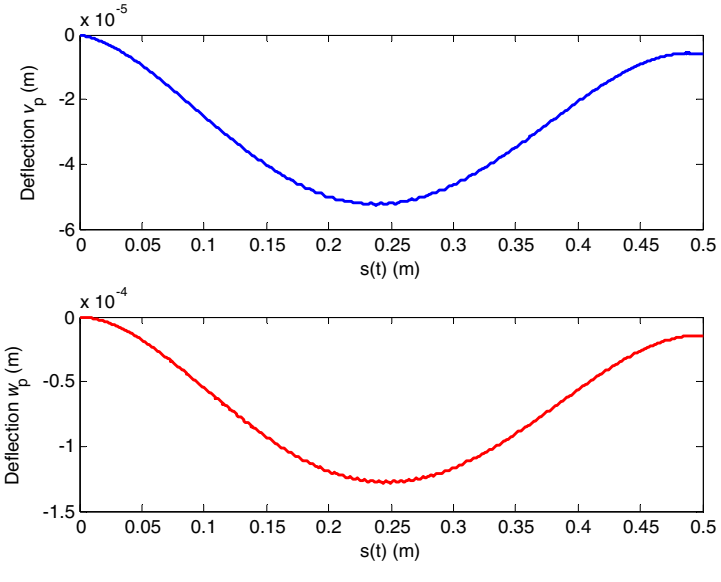

(b)

Fig. 9. Dynamic response of the rotating shaft considering elastically supported boundary conditions subjected to moving load at $u = 2\,\mathrm{m/s}$: (a) Zero initial condition considered and (b) initial static deflection considered.

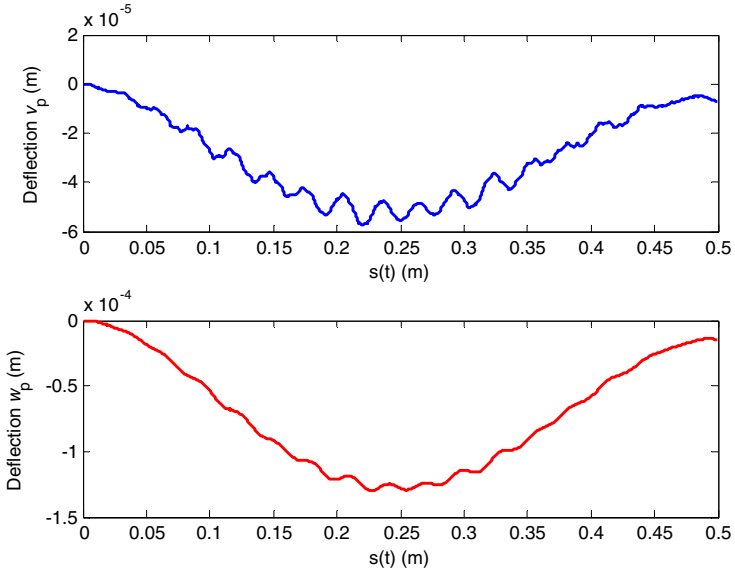

(a)

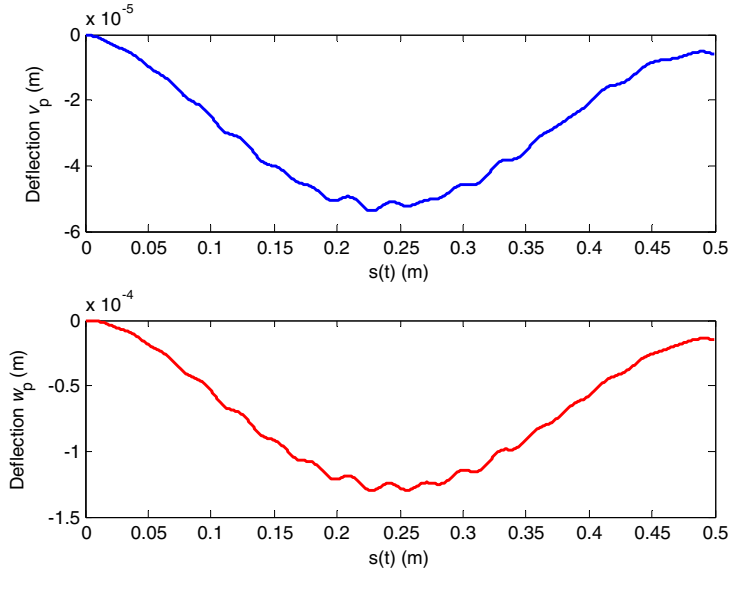

(b)

Fig. 10. Dynamic response of the rotating shaft considering elastically supported boundary conditions subjected to moving load at $u = 10\,\mathrm{m/s}$: (a) Zero initial condition considered and (b) initial static deflection considered.

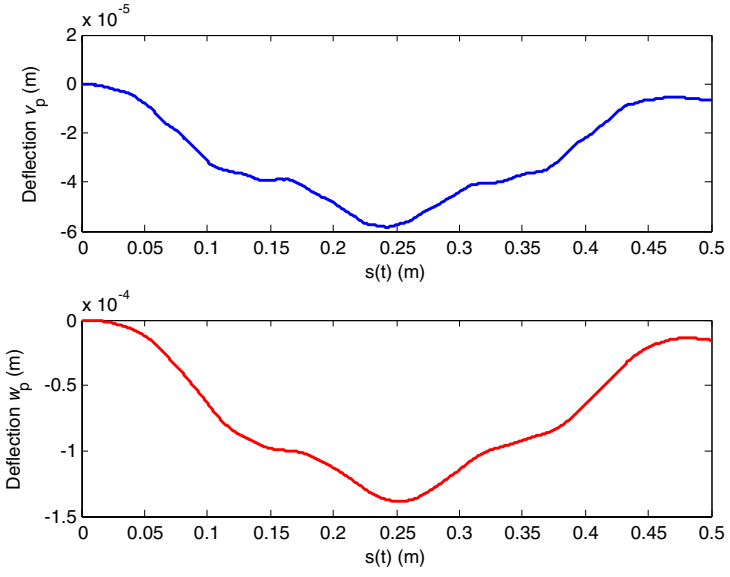

(a)

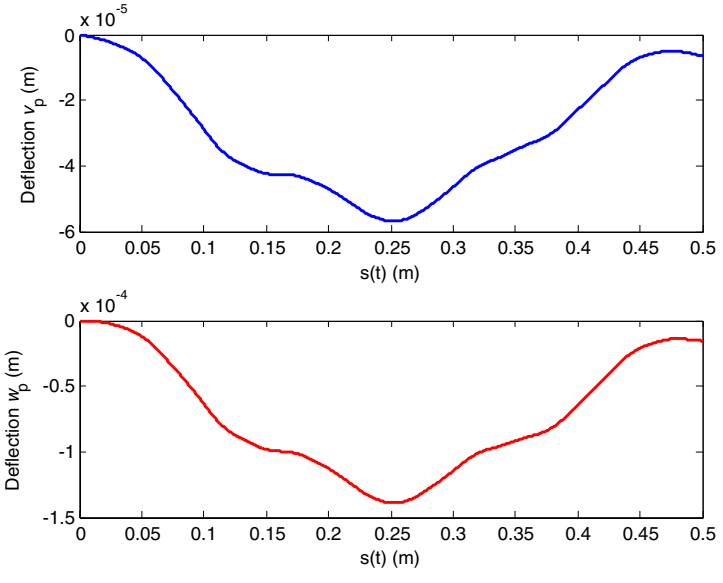

(b)

Fig. 11. Dynamic response of the rotating shaft considering elastically supported boundary conditions subjected to moving load at $u = 50\,\mathrm{m/s}$: (a) Zero initial condition considered and (b) initial static deflection considered.

in Figs. 5(c) and 6(c), Fast Fourier Transform (FFT) of the response w at the middle point of the beam are given, more frequencies are involved in Fig. 5(c). The first six natural frequencies of the work piece with and without considering Gyroscopic effect are also given in Table 2.

As the contributions of the higher frequencies are very small, as can be seen from Figs. 5(c) and 6(c), only the frequencies smaller than 350 Hz are given. By comparing these figures, it can be clearly seen that both for numerical simulation and for real manufacturing process, the initial condition should be taken good care of as they may have a big effect on the final results.

In Fig. 7, the responses of the work piece without considering the bending moment M_z are plotted. The fluctuation with higher frequencies response becomes very small compared with that in Fig. 5, which means that, the bending moment M_z plays a more important role in exciting higher frequency responses than the other two translational forces.

In Figs. 8–11, the responses at different constant moving load velocities from 125 mm/s to 50,000 mm/s are also presented. With a higher velocity, the difference between the response with zero initial conditions and static deflection initial conditions becomes smaller.

4. Conclusions

In this study, a FSM is extended for the vibration analysis of rotating beams with arbitrary boundary conditions as a representation of a work piece being turned. Regardless of the actual boundary conditions involved, each of the displacement solutions is invariably expressed as an accelerated cosine series supplemented by several analytical functions. Thus, this method can be universally applied to beams with arbitrary elastic boundary conditions. In the mathematical model of the rotating work piece on a lathe, the work piece holder is also included and simplified as one lumped mass and inertia. More realistic boundary conditions at the chuck and tail stock are identified as translational and rotational springs based on modal test results. After this, the vibration of the rotating beam with updated boundary conditions subject to moving load is simulated. The numerical results show that the elastic boundary conditions and the moving speed both have some influence on the dynamic response of the rotating beam system subjected to moving load. For moving load problems with elastic boundary conditions, initial conditions should be taken good care of as the dynamic responses could be easily influenced by them, especially when the moving speed is very slow. The presented method can be easily extended to rotating beams with more complex boundary conditions such as more sophisticated supporting systems or even to multi-span beam systems subjected to moving loads.

Acknowledgments

The authors gratefully acknowledge the financial support from National Natural Science Foundation of China (Grant No. 51375104). The first author would also like to thank Professor Xianguo Han from Eastern Liaoning University and Doctor Haiyang Gao from No. 5 Research Institute of China Aerospace Science and Technology Corporation who provided the modal test results. The modeling and computation work is carried out under the supervision of the corresponding author at the University of Liverpool.

Appendix A. Supplemental Information for Eq. (14)

The matrices $\mathbf{M}$, $\mathbf{G}$, $\mathbf{K}$ and $\mathbf{K}_p$, and force vector $\mathbf{F}$ in Eq. (14) can be written as follows:

$$\mathbf{M} = \begin{bmatrix} \left(\begin{array}{l} I_d \int_0^l \boldsymbol{\Psi}'\boldsymbol{\Psi}'^{\mathrm{T}} \mathrm{d}x \\ + \rho A \int_0^l \boldsymbol{\Psi}\boldsymbol{\Psi}^{\mathrm{T}} \mathrm{d}x \end{array}\right) & \mathbf{0} & \mathbf{0} & \mathbf{0} & \mathbf{0} & \mathbf{0} \\ \mathbf{0} & \left(\begin{array}{l} I_d \int_0^l \boldsymbol{\Psi}'\boldsymbol{\Psi}'^{\mathrm{T}} \mathrm{d}x \\ + \rho A \int_0^l \boldsymbol{\Psi}\boldsymbol{\Psi}^{\mathrm{T}} \mathrm{d}x \end{array}\right) & \mathbf{0} & \mathbf{0} & \mathbf{0} & \mathbf{0} \\ \mathbf{0} & \mathbf{0} & m_m & 0 & 0 & 0 \\ \mathbf{0} & \mathbf{0} & 0 & m_m & 0 & 0 \\ \mathbf{0} & \mathbf{0} & 0 & 0 & J_d & 0 \\ \mathbf{0} & \mathbf{0} & 0 & 0 & 0 & J_d \end{bmatrix}, \quad \text{(A.1)}$$

$$\mathbf{G} = \begin{bmatrix} \mathbf{0} & I_p \int_0^l (\boldsymbol{\Psi}'\boldsymbol{\Psi}'^{\mathrm{T}}) \mathrm{d}x & \mathbf{0} & \mathbf{0} & \mathbf{0} & \mathbf{0} \\ -I_p \int_0^l \boldsymbol{\Psi}'\boldsymbol{\Psi}'^{\mathrm{T}} & \mathbf{0} & \mathbf{0} & \mathbf{0} & \mathbf{0} & \mathbf{0} \\ \mathbf{0} & \mathbf{0} & 0 & 0 & 0 & 0 \\ \mathbf{0} & \mathbf{0} & 0 & 0 & 0 & 0 \\ \mathbf{0} & \mathbf{0} & 0 & 0 & 0 & \Omega J_p \\ \mathbf{0} & \mathbf{0} & 0 & 0 & -\Omega J_p & 0 \end{bmatrix}, \quad \text{(A.2)}$$

$$\mathbf{K}=\begin{bmatrix} \mathbf{K}_{\alpha\alpha} & \mathbf{0} & -k_{cy}\boldsymbol{\Psi}|_{x=l} & \mathbf{0} & -K_c\boldsymbol{\Psi}'|_{x=l} & \mathbf{0} \\ \mathbf{0} & \mathbf{K}_{\beta\beta} & \mathbf{0} & -k_{cz}\boldsymbol{\Psi}|_{x=l_i} & \mathbf{0} & -K_c\boldsymbol{\Psi}'|_{x=l} \\ -k_{cy}\boldsymbol{\Psi}^{\mathrm{T}}|_{x=l} & \mathbf{0} & k_{cy} & 0 & 0 & 0 \\ \mathbf{0} & -k_{cz}\boldsymbol{\Psi}^{\mathrm{T}}|_{x=l_i} & 0 & k_{cy} & 0 & 0 \\ -K_c\boldsymbol{\Psi}'^{\mathrm{T}}|_{x=l} & \mathbf{0} & 0 & 0 & K_c & 0 \\ \mathbf{0} & -K_c\boldsymbol{\Psi}'^{\mathrm{T}}|_{x=l} & 0 & 0 & 0 & K_c \end{bmatrix}, \tag{A.3}$$

where

$$\mathbf{K}_{\alpha\alpha}=\left(EI\int_0^l \boldsymbol{\Psi}''\boldsymbol{\Psi}''^{\mathrm{T}}\mathrm{d}x+(k_{x0}\boldsymbol{\Psi}\boldsymbol{\Psi}^{\mathrm{T}}+K_{x0}\boldsymbol{\Psi}'\boldsymbol{\Psi}'^{\mathrm{T}})\Big|_{x=0} + (k_{x1}\boldsymbol{\Psi}\boldsymbol{\Psi}^{\mathrm{T}}+K_{x1}\boldsymbol{\Psi}'\boldsymbol{\Psi}'^{\mathrm{T}})\Big|_{x=l}\right)+(k_{cy}\boldsymbol{\Psi}|_{x=l}\boldsymbol{\Psi}^{\mathrm{T}}|_{x=l}+K_c\boldsymbol{\Psi}'|_{x=l}\boldsymbol{\Psi}'^{\mathrm{T}}|_{x=l}), \tag{A.4}$$

$$\mathbf{K}_{\beta\beta}=\left(EI\int_0^l \boldsymbol{\Psi}''\boldsymbol{\Psi}''^{\mathrm{T}}\mathrm{d}x+(k_{y0}\boldsymbol{\Psi}\boldsymbol{\Psi}^{\mathrm{T}}+K_{y0}\boldsymbol{\Psi}'\boldsymbol{\Psi}'^{\mathrm{T}})\Big|_{x=0} + (k_{y1}\boldsymbol{\Psi}\boldsymbol{\Psi}^{\mathrm{T}}+K_{y1}\boldsymbol{\Psi}'\boldsymbol{\Psi}'^{\mathrm{T}})\Big|_{x=l}\right)+(k_{cz}\boldsymbol{\Psi}|_{x=l_i}\boldsymbol{\Psi}^{\mathrm{T}}|_{x=l_i}+K_c\boldsymbol{\Psi}'|_{x=l}\boldsymbol{\Psi}'^{\mathrm{T}}|_{x=l}), \tag{A.5}$$

$$\mathbf{K}_p(t)=\begin{bmatrix} \mathbf{K}^p_{\alpha\alpha} & \mathbf{0} & \mathbf{0} & \mathbf{0} & \mathbf{0} & \mathbf{0} \\ \mathbf{0} & \mathbf{K}^p_{\beta\beta} & \mathbf{0} & \mathbf{0} & \mathbf{0} & \mathbf{0} \\ \mathbf{0} & \mathbf{0} & 0 & 0 & 0 & 0 \\ \mathbf{0} & \mathbf{0} & 0 & 0 & & 0 \\ \mathbf{0} & \mathbf{0} & 0 & 0 & 0 & 0 \\ \mathbf{0} & \mathbf{0} & 0 & 0 & 0 & 0 \end{bmatrix}, \tag{A.6}$$

$$\mathbf{K}^p_{\alpha\alpha}=-P_x\int_s^l \boldsymbol{\Psi}'\boldsymbol{\Psi}'^{\mathrm{T}}\mathrm{d}x, \tag{A.7}$$

$$\mathbf{K}^p_{\beta\beta}=-P_x\int_s^l \boldsymbol{\Psi}'\boldsymbol{\Psi}'^{\mathrm{T}}\mathrm{d}x, \tag{A.8}$$

$$\mathbf{F}=\{P_y\boldsymbol{\Psi}^{\mathrm{T}}|_{x=s}-P_x r\boldsymbol{\Psi}'^{\mathrm{T}}|_{x=s},P_z\boldsymbol{\Psi}^{\mathrm{T}}|_{x=s},0,0,0,0\}^{\mathrm{T}}. \tag{A.9}$$

References

1. M. I. Friswell, *Dynamics of Rotating Machines*, Cambridge aerospace series (Cambridge University Press, Cambridge, 2010).

2. Y. B. Yang, J. Yau and Y. Wu, *Vehicle-Bridge Interaction Dynamics: With Application to High-Speed Railways* (World Scientific, Singapore, 2004).
3. J. D. Yau, Y. S. Wu and Y. B. Yang, Impact response of bridges with elastic bearings to moving loads, *J. Sound. Vib.* **248**(1) (2001) 9–30.
4. H. Ouyang and M. J. Wang, Dynamics of a rotating shaft subject to a three-directional moving load, *J. Vib. Acoust.* **129**(3) (2007) 386–389.
5. R. Katz, C. W. Lee, A. G. Ulsoy and R. A. Scott, The dynamic-response of a rotating shaft subject to a moving load, *J. Sound. Vib.* **122**(1) (1988) 131–148.
6. S. F. Xiao and M. Yang, Nonlinear dynamic modeling, instability and post-buckling analysis of a rotating beam with a flexible support, *Int. J. Struct. Stab. Dyn.* **6**(4) (2006) 475–491.
7. C. F. J. Kuo, H. M. Tu, V. Q. Huy and C. H. Liu, Dynamic stability analysis and vibration control of a rotating elastic beam connected with an end mass, *Int. J. Struct. Stab. Dyn.* **13**(3) (2013) 1250066-1–24.
8. S. C. Huang and B. S. Hsu, Resonant phenomena of a rotating cylindrical shell subjected to a harmonic moving load, *J. Sound. Vib.* **136**(2) (1990) 215–228.
9. Y. H. Lin and M. W. Trethewey, Finite element analysis of elastic beams subjected to moving dynamic loads, *J. Sound. Vib.* **136**(2) (1990) 323–342.
10. A. Argento and R. A. Scott, Dynamic response of a rotating beam subjected to an accelerating distributed surface force, *J. Sound. Vib.* **157**(2) (1992) 221–231.
11. A. Argento, A spinning beam subjected to a moving deflection dependent load: Part I: response and resonance, *J. Sound. Vib.* **182**(4) (1995) 595–615.
12. H. P. Lee, Dynamic response of a rotating timoshenko shaft subject to axial forces and moving loads, *J. Sound. Vib.* **181**(1) (1995) 169–177.
13. S. H. Zibdeh and S. H. Juma, Dynamic response of a rotating beam subjected to a random moving load, *J. Sound. Vib.* **223**(5) (1999) 741–758.
14. F. M. A. El-Saeidy, Finite-element dynamic analysis of a rotating shaft with or without nonlinear boundary conditions subject to a moving load, *Nonlin. Dyn.* **21**(4) (2000) 377–407.
15. Y. J. Wang and Q. C. Wei, Interaction response of train loads moving over a two-span continuous beam, *Int. J. Struct. Stab. Dyn.* **29**(7–8) (2006) 648–654.
16. C. K. Chen and Y. M. Tsao, A stability analysis of regenerative chatter in turning process without using tailstock, *Int. J. Adv. Manuf. Tech.* **29**(7–8) (2006) 648–654.
17. H. Ouyang and M. Wang, A dynamic model for a rotating beam subjected to axially moving forces. *J. Sound. Vib.* **308**(3–5) (2007) 674–682.
18. A. Ganguli, A. Deraemaeker and A. Preumont, Regenerative chatter reduction by active damping control, *J. Sound. Vib.* **300**(3–5) (2007) 847–862.
19. T. Insperger, D. A. W. Barton and G. Stepan, Criticality of Hopf bifurcation in state-dependent delay model of turning processes, *Int. J. Nonlin. Mech.* **43**(2) (2008) 140–149.
20. G. Litak, S. Schubert and G. Radons, Nonlinear dynamics of a regenerative cutting process, *Nonlinear. Dyn.* **69**(3) (2012) 1255–1262.
21. L. Dai and J. Wang, The effects of workpiece deflection and motor features on quality of machining process — nonlinear vibrations analysis, *J. Vib. Control.* **13**(5) (2007) 557–582.
22. X. G. Han, H. Ouyang, M. Wang, N. Hassan and Y. Mao, Self-excited vibration of workpieces in a turning process, *P. I. Mech. Eng. C-J. Mech. Eng. Sci.* **226**(C8) (2012) 1958–1970.
23. W. L. Li, Free vibrations of beams with general boundary conditions, *J. Sound. Vib.* **237**(4) (2000) 709–725.

24. J. T. Du, W. L. Li, Z. G. Liu, T. Yang and G. Jin, Free vibration of two elastically coupled rectangular plates with uniform elastic boundary restraints, *J. Sound. Vib.* **330**(4) (2011) 788–804.
25. M. I. Friswell and J. E. Mottershead, *Finite Element Model Updating in Structural Dynamics*, Solid Mechanics and Its Applications (Kluwer Academic Publishers, Boston, 1995).